2022 IEEE 23rd International Workshop on Signal Processing Advances in Wireless Communication (SPAWC) | 978-1-6654-9455-7/22/$31.00 ©2022 IEEE | DOI: 10.1109/SPAWC51304.2022.9833962

Parametrization of High-Rank Line-of-Sight MIMO Channels with Reflected Paths

Yaqi Hu, Mingsheng Yin, Sundeep Rangan, Marco Mezzavilla
NYU Tandon School of Engineering, Brooklyn, NY, USA

***Abstract*—High-rank line-of-sight (LOS) MIMO systems have attracted considerable attention for millimeter wave and THz communications. The small wavelengths in these frequencies enable spatial multiplexing with massive data rates at long distances. Such systems are also being considered for multi-path non-LOS (NLOS) environments. In these scenarios, standard channels models based on plane waves cannot capture the curvature of each wave front necessary to model spatial multiplexing. This work presents a novel and simple multi-path wireless channel parametrization where each path is replaced by a LOS path with a reflected image source. The model fully captures the spherical nature of each wave front and uses only two additional parameters relative to the standard plane wave model. Moreover, the parameters can be easily captured in standard ray tracing. The accuracy of the approach is demonstrated on detailed ray tracing simulations at $28\,\mathrm{GHz}$ and $140\,\mathrm{GHz}$ in a dense urban area.**

***Index Terms*—MmWave, THz communication, LOS MIMO, channel models**

I. Introduction

Line-of-sight (LOS) multi-input multi-output (MIMO) systems [1], [2], [3] have emerged as valuable technology for the millimeter wave (mmWave) and terahertz (THz) frequencies. The concept is to operate communication links at a transmitter-receiver (TX-RX) separation, R, less than so-called Rayleigh distance,

$$R < R_{\text{rayleigh}} \approx \frac{2d^2}{\lambda}, \tag{1}$$

where d is the total aperture of the TX and RX arrays and λ is the wavelength. In this regime, links can support multiple spatial streams even with a single LOS path [4]. LOS MIMO is particularly valuable in the mmWave and THz frequencies, where the wavelength λ is small and hence the Rayleigh distance — which sets the maximum range of such systems — is large. Indeed, there have been several demonstrations in the mmWave spectrum [5], and, with the advancement of communication systems in the THz and sub-THz bands [6], there has been growing interest in high-rank LOS MIMO in higher frequencies as well [7] – see, for example, some recent work at $140\,\mathrm{GHz}$ [8], [9].

Many applications for such LOS MIMO systems are envisioned as operating in NLOS settings. For example, in mid-haul and backhaul applications – a key target application for sub-THz systems [9], [10], [11] – NLOS paths may be present from ground clutter when serving street-level radio units. In this work, we will use the term *wide aperture MIMO*, instead of *LOS MIMO*, since we are interested in cases where the systems operate in such NLOS settings.

The authors were supported by NSF grants 1952180, 1925079, 1564142, 1547332, the SRC, OPPO, and the industrial affiliates of NYU WIRELESS. The work was also supported by Remcom that provided the Wireless Insite software.

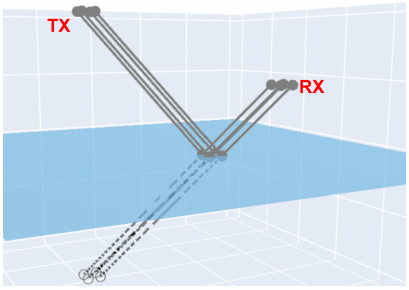

Fig. 1: The proposed reflection model replaces each reflected path with a LOS path with a mirror image source. The spherical wave from this source can then be easily modeled for arbitrarily wide aperture arrays.

Evaluating wide aperture systems in NLOS environments requires accurate channel models to describe multi-path propagation. Conventional statistical multipath models, such as those used by 3GPP [12], describe each path as a propagating plane wave with a gain, delay, and directions of arrival and departure. Under this standard plane wave approximation (PWA), the MIMO channel response can be computed for any array geometries at the TX and RX [13]. However, the PWA model is not valid when the TX-RX separation is below the Rayleigh distance (i.e., not in the far-field), since the curvature of each wavefront becomes important. While spherical wave models are well-understood for single LOS path channels [14], there are currently few techniques to model them in NLOS multi-path settings.

In this work, we present a simple parameterization for multipath channels that captures the full spherical nature of each wavefront. The model is valid for both LOS paths as well as NLOS path arising from arbitrary numbers of specular reflections. The main concept is that, in such environments, each NLOS path can be replaced by a LOS path where the TX location is replaced by a virtual image source from the reflection on the source – See Fig. 1. This idea is the same concept that underlies the method of images in ray tracing [15]. Our main contribution here shows that the propagation

from each such image can be parametrized by two additional parameters relative to the plane wave model. We call the paramerization the *reflection model*, or RM.

In addition, we show how these parameters can be extracted for site-specific evaluations via ray tracing. Analyzing wide aperture systems with ray tracing typically requires running the simulations between each transmitter and receiver element pair, which can be computationally expensive when the number of elements is large. In addition, the ray tracing must be repeated for different antenna geometries or orientations, making site planning and capacity evaluation time consuming. In contrast, we show how the full parameters for the RM can be computed from ray tracing at only two locations near the array centers.

II. Plane Wave Approximations for Multi-Path Channels

We begin by reviewing the standard plane wave multi-path channel models using the perspective in [14]. Consider a wireless channel from a TX locations $\boldsymbol{x}^t \in \mathcal{A}^t$ to RX locations $\boldsymbol{x}^r \in \mathcal{A}^r$, where $\mathcal{A}^t$ and $\mathcal{A}^r \subset \mathbb{R}^d$ are some regions that can contain the elements in the TX and RX arrays. We will consider both planar models with $d = 2$ and so-called 3D models with $d = 3$. The channel is typically described by a set of discrete paths representing the routes of propagation from the TX to RX locations. For MIMO processing, one commonly assumes that the complex channel gain for each path from is given by

$$H = g \exp\left(\frac{2\pi i}{\lambda} d(\boldsymbol{x}^r, \boldsymbol{x}^t)\right), \tag{2}$$

where g is a complex nominal channel gain (assumed to be approximately constant over the region), $d(\boldsymbol{x}^r, \boldsymbol{x}^t)$ is the propagation distance of the path and λ is the wavelength [13]. We will call $d(\boldsymbol{x}^r, \boldsymbol{x}^t)$ the *path distance function* for the path.

Describing the gain and path distance function for each path is sufficient to compute the response for arbitrary TX and RX arrays. For example, suppose that the TX array has $N_{\rm tx}$ elements at locations $x_n^t \in \mathcal{A}^t$, $n = 1, \ldots, N_{\rm tx}$ and the RX array has elements at locations $x_m^r \in \mathcal{A}^r$, $m = 1, \ldots, N_{\rm rx}$. Then, the narrowband frequency response is the matrix with coefficients

$$H_{mn}(f) = \sum_{\ell=1}^{L} g_\ell \exp\left(\frac{2\pi i f}{c} d_\ell(\boldsymbol{x}_m^r, \boldsymbol{x}_n^t)\right), \tag{3}$$

where f is the frequency, c is the speed of light, L is the number of paths, and, for each path ℓ, g_ℓ is its gain and $d_\ell(\boldsymbol{x}^r, \boldsymbol{x}^t)$ is its path distance function Hence, if we can find the gain g_ℓ and path distance function $d_\ell(\boldsymbol{x}^r, \boldsymbol{x}^t)$ for each path, we can compute the wideband MIMO channel response.

The main challenge is how to model the path distance function $d_\ell(\boldsymbol{x}^r, \boldsymbol{x}^t)$ as a function of $\boldsymbol{x}^r$ and $\boldsymbol{x}^t$. In a LOS path, the path distance function is simply the Euclidean distance

$$d(\boldsymbol{x}^r, \boldsymbol{x}^t) = \|\boldsymbol{x}^r - \boldsymbol{x}^t\|. \tag{4}$$

For NLOS paths, the distance function is usually approximated under the assumption that the propagation in each path are plane waves. Specifically, suppose that $\boldsymbol{x}_0^r$ and $\boldsymbol{x}_0^t$ are some reference locations for the RX and TX. For example, these points could be the centroids of the arrays. Now, for small displacements $\boldsymbol{x}^t - \boldsymbol{x}_0^t$ and $\boldsymbol{x}^r - \boldsymbol{x}_0^r$, one often assumes a plane wave approximation (PWA)

$$d(\boldsymbol{x}^r, \boldsymbol{x}^t) \approx c\tau + (\boldsymbol{u}^r)^{\mathsf{T}}(\boldsymbol{x}_0^r - \boldsymbol{x}^r) + (\boldsymbol{u}^t)^{\mathsf{T}}(\boldsymbol{x}_0^t - \boldsymbol{x}^t), \tag{5}$$

where c is the speed of light, τ is the time of flight between the nominal points $\boldsymbol{x}_0^r$ and $\boldsymbol{x}_0^t$, and $\boldsymbol{u}^r$ and $\boldsymbol{u}^t$ are unit vectors in $\mathbb{R}^d$ representing the directions of arrival and departure of the path. We will call (5) the *PWA model*.

In the LOS case (4), the parameters for the PWA model (5) are

$$\tau = \frac{1}{c}\|\boldsymbol{x}_0^r - \boldsymbol{x}_0^t\| \tag{6a}$$

$$\boldsymbol{u}^r = \frac{\boldsymbol{x}^t - \boldsymbol{x}^r}{c\tau}, \quad \boldsymbol{u}^t = \frac{\boldsymbol{x}^r - \boldsymbol{x}^t}{c\tau}. \tag{6b}$$

Typically, we express the directions $\boldsymbol{u}^r$ and $\boldsymbol{u}^t$ in spherical coordinates. For $d = 3$, we can write these unit vectors as

$$\boldsymbol{u}^r = (\cos(\phi^r)\cos(\theta^r), \sin(\phi^r)\cos(\theta^r), \sin(\theta^r)) \tag{7a}$$

$$\boldsymbol{u}^t = (\cos(\phi^t)\cos(\theta^t), \sin(\phi^t)\cos(\theta^t), \sin(\theta^t)), \tag{7b}$$

where ϕ^r, ϕ^t are the azimuth AoA and AoD and θ^r, θ^t are the elevation AoA and AoD. Thus, each path ℓ can be described by six parameters:

$$\psi_\ell = (g_\ell, \tau_\ell, \phi_\ell^r, \theta_\ell^r, \phi_\ell^t, \theta_\ell^t), \tag{8}$$

where τ_ℓ is the absolute propagation delay, and g_ℓ is the path gain. The PWA model (5) thus has clear benefits: it is easy to evaluate, it is geometrically interpretable and accurate when the total array aperture is small. The main disadvantage is that it becomes inaccurate when the array aperture is large and higher-order terms of the displacements $\boldsymbol{x}^r - \boldsymbol{x}_0^r$ and $\boldsymbol{x}^t - \boldsymbol{x}_0^t$ become significant. In particular, the PWA model always predicts that each path contributes at most one spatial rank. But, for wide aperture arrays, the channel can have higher rank even with a single path.

In contrast, the path distance function (4) is exact for arbitrary displacements. However, this model is only valid for LOS paths. The question is whether there is a model for the path distance function that is exact for arbitrary array sizes and applies in NLOS settings.

III. High Order Modeling in NLOS Channels

Our main result provides a simple parametrization of the path distance functions for paths with arbitrary numbers of specular reflections. We do not consider diffractions or scattering. However, we will show in simulations below that, even with diffractions and transmission losses such as foliage, the model performs well.

To state the result, let $\mathcal{A}^t$ and $\mathcal{A}^r \subset \mathbb{R}^d$ be regions of space. Suppose that for every TX location $\boldsymbol{x}^t \in \mathcal{A}^t$ and RX location $\boldsymbol{x}^r \in \mathcal{A}^r$ there is a path that has a constant set of

reflecting surfaces. In this case, we will say the path *has constant interactions* over the regions $\mathcal{A}^t$ and $\mathcal{A}^r$. Let $R_z(\phi)$, $R_y(\theta)$ and $R_x(\gamma)$ be the rotation matrices around the z, y and x axes:

$$\boldsymbol{R}_z(\phi) := \begin{bmatrix} \cos(\phi) & -\sin(\phi) & 0 \\ \sin(\phi) & \cos(\phi) & 0 \\ 0 & 0 & 1 \end{bmatrix}, \tag{9a}$$

$$\boldsymbol{R}_y(\theta) := \begin{bmatrix} \cos(\theta) & 0 & \sin(\theta) \\ 0 & 1 & 0 \\ -\sin(\theta) & 0 & \cos(\theta) \end{bmatrix} \tag{9b}$$

$$\boldsymbol{R}_x(\gamma) := \begin{bmatrix} 1 & 0 & 0 \\ 0 & \cos(\gamma) & -\sin(\gamma) \\ 0 & \sin(\gamma) & \cos(\gamma) \end{bmatrix} \tag{9c}$$

Also, for $s = \pm 1$, let $\boldsymbol{Q}_z(s)$ be the reflection in the z-axis:

$$\boldsymbol{Q}_z(s) := \begin{bmatrix} 1 & 0 & 0 \\ 0 & 1 & 0 \\ 0 & 0 & s \end{bmatrix}. \tag{10}$$

Theorem 1: Suppose a path has K specular reflections with constant interactions from regions $\mathcal{A}^t$ to $\mathcal{A}^r \subset \mathbb{R}^d$. Let $\boldsymbol{x}_0^t \in \mathcal{A}^t$ and $\boldsymbol{x}_0^r \in \mathcal{A}^r$ be arbitrary points in these regions. Then, if $d = 3$, there exists parameters

$$(\tau, \phi^r, \theta^r, \phi^t, \theta^t, \gamma^t, s) \tag{11}$$

where

$$s = \begin{cases} 1 & \text{if } K \text{ is odd} \\ -1 & \text{if } K \text{ is even,} \end{cases} \tag{12}$$

and for all $\boldsymbol{x}^r \in \mathcal{A}^r$ and $\boldsymbol{x}^t \in \mathcal{A}^t$, the total path distance is

$$d(\boldsymbol{x}^r, \boldsymbol{x}^t) = \Big\| c\tau \boldsymbol{e}_x + \boldsymbol{R}_y(\theta^r)\boldsymbol{R}_z(-\phi^r)(\boldsymbol{x}_0^r - \boldsymbol{x}^r) + \boldsymbol{Q}_z(s)\boldsymbol{R}_x(\gamma^t)\boldsymbol{R}_y(\theta^t)\boldsymbol{R}_z(-\phi^t)(\boldsymbol{x}_0^t - \boldsymbol{x}^t) \Big\|. \tag{13}$$

Proof: For space considerations, we place the proof in a full paper [16]. The basic idea is to replace the reflected path with a LOS path with a reflected image – See Fig. 1. The mirror image is an orthogonal and affine transformation of the original point. The parameterization (13) can then be found by parameterizing the orthogonal transformations by their Givens rotations. ■

The distance function (13) has a simple geometric interpretation: The distance of any reflected path is identical to the distance on a LOS path but with the TX and RX frames of reference being rotated. The RX rotation is described by elevation and azimuth angles and the TX rotation is described by roll, elevation and azimuth angles γ^t, θ^t and ϕ^t.

The total path parameters for each path ℓ will be:

$$(g_\ell, \tau_\ell, \phi_\ell^r, \theta_\ell^r, \phi_\ell^t, \theta_\ell^t, \gamma_\ell^t, s_\ell). \tag{14}$$

In comparison to (6), there is one additional binary parameter $s_\ell = \pm 1$ and one additional angle γ_ℓ^t. We have thus found a concise parametrization of the distance function that is exact and is valid for all paths with arbitrary reflections. We will call the parameterization of each path by the parameters (14) the *reflection model* (RM).

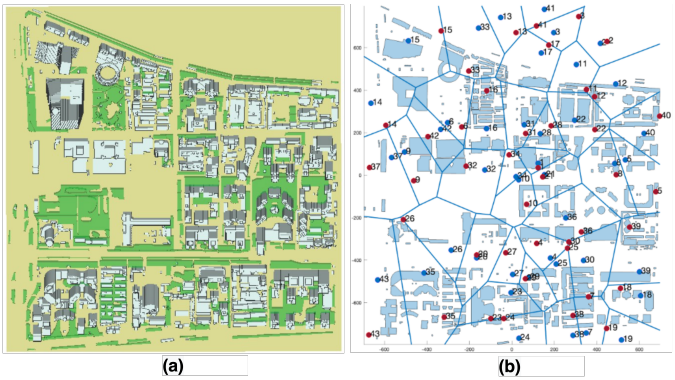

Fig. 2: (a) An example of the ray tracing environment: a section of Beijing city. Foliage areas are indicated by the green blocks. (b) The distribution of reference TX and RX pairs. The transmitters and receivers are dropped randomly by implementing a Voronoi partition within our partial Beijing area.

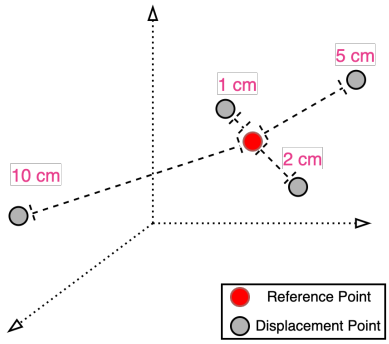

Fig. 3: Around each reference location $(\boldsymbol{x}_0^r, \boldsymbol{x}_0^t)$, we generated displaced locations at random 3D locations $(\boldsymbol{x}_i^r, \boldsymbol{x}_i^t)$ at distances: 1 cm, 2 cm, 5 cm, 10 cm, 50 cm and 100 cm.

IV. Fitting the Reflection Model with Ray Tracing

A benefit of the PWA model is that one typically only needs to run ray tracing between the reference TX and RX locations $\boldsymbol{x}_0^t$ and $\boldsymbol{x}_0^r$. Then, for any elements close to the reference locations, the path distance and phase offset of the path can be computed from (5). However, this approach is not valid for wide aperture arrays where the displacements $\boldsymbol{x}^t - \boldsymbol{x}_0^t$ and $\boldsymbol{x}^r - \boldsymbol{x}_0^r$ are large. In these cases, one must typically run ray tracing separately for each pair of TX and RX elements to capture the full MIMO response accurately. Hence, if there are N_{tx} and N_{rx} elements on the the TX and RX arrays, the computational complexity grows by $N_{\text{rx}}N_{\text{tx}}$.

In contrast, we show that the parameters of the reflection model (14) can be captured with only *three* ray tracing simulations: One between a reference TX-RX pair $(\boldsymbol{x}_0^t, \boldsymbol{x}_0^r)$, and two between two randomly displaced TX-RX pair $(\boldsymbol{x}_1^t, \boldsymbol{x}_1^r)$, $(\boldsymbol{x}_2^t, \boldsymbol{x}_2^r)$. The procedure is as follows: First, running the ray tracing on the reference pair$(\boldsymbol{x}_0^t, \boldsymbol{x}_0^r)$ provides the parameters (6). Also, s can be determined from the number of reflections K in (12). So, we only need to find γ_ℓ for each path. Ray trac-

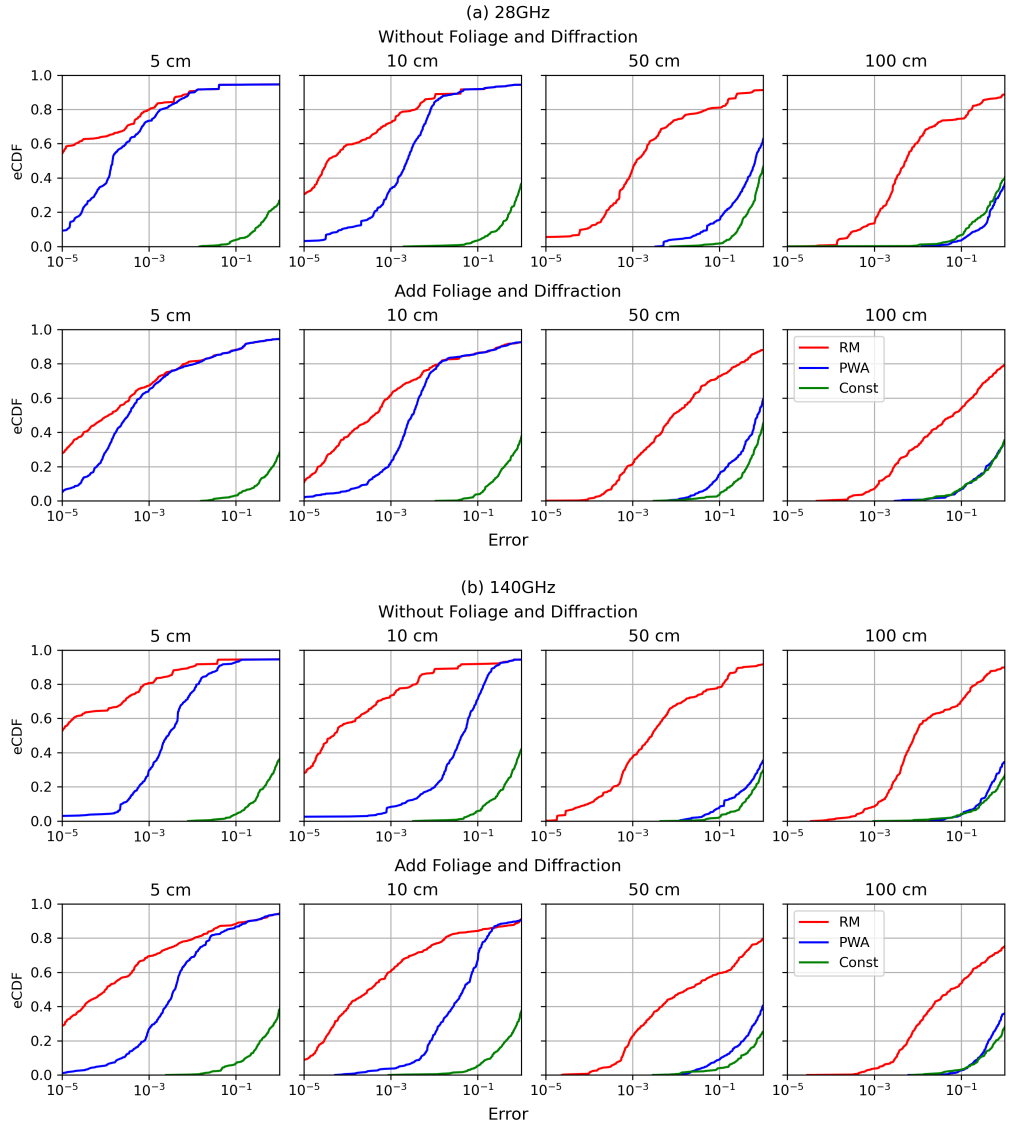

Fig. 4: eCDF plot for the error of estimated channel gain in the randomized directions at different distances. The displacement distances are set to $5\,\mathrm{cm}$, $10\,\mathrm{cm}$, $50\,\mathrm{cm}$, and $100\,\mathrm{cm}$. (a) $28\,\mathrm{GHz}$; (b) $140\,\mathrm{GHz}$.

ing also provides the total path distances $d(\boldsymbol{x}_2^r, \boldsymbol{x}_2^t)$, $d(\boldsymbol{x}_1^r, \boldsymbol{x}_1^t)$ and $d(\boldsymbol{x}_0^r, \boldsymbol{x}_0^t)$. Using (13), the difference in distances

$$d(\boldsymbol{x}_1^r, \boldsymbol{x}_1^t) - d(\boldsymbol{x}_0^r, \boldsymbol{x}_0^t), \tag{15a}$$

$$d(\boldsymbol{x}_2^r, \boldsymbol{x}_2^t) - d(\boldsymbol{x}_0^r, \boldsymbol{x}_0^t) \tag{15b}$$

are the functions of the parameters (14). Since all the parameters in (14) are known except for γ_ℓ, we can solve for γ_ℓ from the difference (15). Then, all the parameters in (14) are known and the path distances can be computed between any two TX and RX elements without any further ray tracing. Details can be found in the full paper [16].

V. Validation in a Urban Environment

We validate the methods on a ray tracing simulation of a 1650×1440 square meter area of a dense urban environment of Beijing, China, as shown in Fig. 2. The identical ray tracing environment was used in the channel modeling work [17]. Within this area, we selected $N = 43$ TX and RX pairs spaced within $200\,\mathrm{m}$. We call each of these pairs the *reference locations*. For each such reference pair $(\boldsymbol{x}_0^r, \boldsymbol{x}_0^t)$, we also generated $M = 6$ random *displaced* locations $(\boldsymbol{x}_i^r, \boldsymbol{x}_i^t)$, $i = 1, \ldots, M$ with distances from $1\,\mathrm{cm}$ to $100\,\mathrm{cm}$ from the reference location. Let $H_i(f)$ denote the complex channel from the $\boldsymbol{x}_i^t$ to $\boldsymbol{x}_i^r$ at frequency f. The "true" value of this channel can be computed via ray tracing. Specifically, we run ray tracing at some reference frequency f_0 between the reference and displaced TX-RX pairs $(\boldsymbol{x}_i^t, \boldsymbol{x}_i^r)$, $i = 0, \ldots, M$. Then, the complex channel gain at any other frequency f is given by

$$H_i(f) = \sum_{\ell=1}^{L_i} g_{\ell i} e^{2\pi j (f - f_0)\tau_{\ell i}}, \tag{16}$$

where L_i is the number of paths between $\boldsymbol{x}_i^t$ and $\boldsymbol{x}_i^r$; and for path ℓ, $g_{\ell i}$ is the complex gain of the path, and $\tau_{\ell i}$ is its delay.

We wish to see how well different models can predict the channels $H_i(f)$ between the displaced TX-RX pairs $(\boldsymbol{x}_i^r, \boldsymbol{x}_i^t)$ from information near the reference TX-RX pair $(\boldsymbol{x}_0^r, \boldsymbol{x}_0^t)$. We compare three methods:

- *Constant model*: $\widehat{H}_i(f) = H_0(f)$ where we assume that the channel does not change from the reference location.
- *PWA model:* The estimate is computed from

$$\widehat{H}_i(f) = \sum_{\ell=1}^{L_0} g_{\ell 0} e^{2\pi j (f d_{\ell i}/c - \tau_{\ell 0} f_0)}, \tag{17}$$

  where $d_{\ell i}$ is the estimate of the distance $d(\boldsymbol{x}_i^r, \boldsymbol{x}_i^t)$ from the PWA model (5).
- *Reflection model (RM)*: The estimate (17) where the distances $d_{\ell i}$ are the estimates of the distances $d(\boldsymbol{x}_i^r, \boldsymbol{x}_i^t)$ computed from the reflection model (13).

For the reference model, the parameters were extracted as described in Section IV using the reference location and the displacement at $1\,\mathrm{cm}$.

Similar to [18], we performed the validation on two bands: $28\,\mathrm{GHz}$ with a bandwidth of $400\,\mathrm{MHz}$, and $140\,\mathrm{GHz}$ with a bandwidth of $2\,\mathrm{GHz}$. On each link, the true and estimated channels were computed at the reference and displaced locations at ten random frequencies within the bandwidth. All ray tracing was performed using Wireless Insite by Remcom [19]. The source code and data for the validation process can be found at [20].

We compute the normalized mean squared errors:

$$\epsilon_i(f) := \frac{\left|\widehat{H}_i(f) - H_i(f)\right|^2}{E_0}, \quad E_0 := \sum_{\ell=1}^{L_0} |g_{\ell 0}|^2 \tag{18}$$

which represents the channel estimate error relative to the average wideband received channel energy.

Fig. 4 plot the empirical cumulative distribution function of the error (18) in both $28\,\mathrm{GHz}$ and $140\,\mathrm{GHz}$. As expected, for all models, as the displacement from the reference location is increased, the error increases since we are trying to extrapolate the channel from the reference. What is important is that the reflection model obtains dramatically lower errors at high displacements. For example, even at a $100\,\mathrm{cm}$ displacement, the median relative error of the RM is less that 10^{-2}, thus enabling accurate calculation of the MIMO matrix terms. In contrast, the relative error is > 1 for the PWA and constant model. Interestingly, although the proposed reflection model is only theoretically correct for fully specular reflections, we see that low errors are obtainable even with foliage and diffraction.

VI. Conclusions

We have presented a simple parameterization for multipath wireless channels that captures the spherical wavefront of each path. The parameterization requires only two additional parameters relative to standard plane wave models. The parameters can be found easily from ray tracing. The work will enable easier evaluation of mmWave and THz backhaul in site-specific settings. In addition, a natural next step is to develop statistical channel models, such as those used by 3GPP [12], or machine learning methods [17], that describe the distribution of these paramters in common environments.

References

[1] F. Bohagen, P. Orten, and G. Oien, "Construction and capacity analysis of high-rank line-of-sight MIMO channels," in *IEEE Wireless Communications and Networking Conference, 2005*, vol. 1, 2005, pp. 432–437.

[2] I. Sarris and A. R. Nix, "Design and performance assessment of high-capacity MIMO architectures in the presence of a line-of-sight component," *IEEE Transactions on Vehicular Technology*, vol. 56, no. 4, pp. 2194–2202, 2007.

[3] M. Matthaiou, D. I. Laurenson, and C.-X. Wang, "Capacity study of vehicle-to-roadside MIMO channels with a line-of-sight component," in *Proc. IEEE Wireless Communications and Networking Conference*, 2008, pp. 775–779.

[4] J. Winters, "On the capacity of radio communication systems with diversity in a rayleigh fading environment," *IEEE journal on selected areas in communications*, vol. 5, no. 5, pp. 871–878, 1987.

[5] C. Sheldon, E. Torkildson, M. Seo, C. P. Yue, U. Madhow, and M. Rodwell, "A 60GHz line-of-sight 2x2 MIMO link operating at 1.2 Gbps," in *Proc. IEEE Antennas and Propagation Society International Symposium*, 2008, pp. 1–4.

[6] T. Kürner and S. Priebe, "Towards THz communications-status in research, standardization and regulation," *Journal of Infrared, Millimeter, and Terahertz Waves*, vol. 35, no. 1, pp. 53–62, 2014.

[7] S. Singh, H. Tran, and T. Le, "Challenges in LoS terahertz MIMO," in *2019 IEEE Global Communications Conference (GLOBECOM)*. IEEE, 2019, pp. 1–5.

[8] A. U. Zaman, S. Rahiminezad, T. Eriksson, S. Faijana, and P. Enoksson, "140 GHz planar gap waveguide array antenna for line of sight (LOS) MIMO backhaul links," in *12th European Conference on Antennas and Propagation (EuCAP 2018)*. IET, 2018, pp. 1–4.

[9] M. Sawaby, B. Grave, C. Jany, C. Chen, S. Kananian, P. Calascibetta, F. Gianesello, and A. Arbabian, "A Fully Integrated 32 Gbps 2x2 LoS MIMO Wireless Link with UWB Analog Processing for Point-to-Point Backhaul Applications," in *2020 IEEE Radio Frequency Integrated Circuits Symposium (RFIC)*. IEEE, 2020, pp. 107–110.

[10] G. Gougeon, Y. Corre, M. Z. Aslam, S. Bicaïs, and J.-B. Doré, "Assessment of sub-THz mesh backhaul capabilities from realistic modelling at the PHY layer," in *Proc. IEEE European Conference on Antennas and Propagation (EuCAP)*, 2020, pp. 1–5.

[11] S. R. Chintareddy, M. Mezzavilla, S. Rangan, and M. Hashemi, "A preliminary assessment of midhaul links at 140 GHz using ray-tracing," in *Proceedings of the 5th ACM Workshop on Millimeter-Wave and Terahertz Networks and Sensing Systems*, 2021, pp. 25–30.

[12] 3GPP Technical Report 38.901, "Study on channel model for frequencies from 0.5 to 100 GHz (Release 16)," Dec. 2019.

[13] R. W. Heath Jr. and A. Lozano, *Foundations of MIMO Communication*. Cambridge University Press, 2018.

[14] F. Bohagen, P. Orten, and G. E. Oien, "On spherical vs. plane wave modeling of line-of-sight mimo channels," *IEEE Transactions on Communications*, vol. 57, no. 3, pp. 841–849, 2009.

[15] Z. Yun and M. F. Iskander, "Ray tracing for radio propagation modeling: Principles and applications," *IEEE Access*, vol. 3, pp. 1089–1100, 2015.

[16] Y. Hu, M. Yin, M. Mezzavilla, and S. Rangan, "Parametrization of Line-of-Sight MIMO Channels for Reflected Paths," *arxiv pre-print*, 2022.

[17] W. Xia, S. Rangan, M. Mezzavilla, A. Lozano, G. Geraci, V. Semkin, and G. Loianno, "Millimeter wave channel modeling via generative neural networks," in *Proc. IEEE Globecom Workshops.*, 2020, pp. 1–6.

[18] P. Skrimponis, S. Dutta, M. Mezzavilla, , S. Rangan, S. H. Mirfarshbafan, C. Studer, J. Buckwalter, and M. Rodwell, "Power Consumption Analysis for Mobile MmWave and Sub-THz Receivers," in *Proc. IEEE 6G Wireless Summit*, 2020.

[19] "Remcom (accessed on March 10 2022)," available on-line at `https://www.remcom.com/`.

[20] "Wide aperture MIMO in NLOS github repository," available on-line at `https://github.com/nyu-wireless/wide-aperture-MIMO`.